



저작자표시-비영리-변경금지 2.0 대한민국

이용자는 아래의 조건을 따르는 경우에 한하여 자유롭게

- 이 저작물을 복제, 배포, 전송, 전시, 공연 및 방송할 수 있습니다.

다음과 같은 조건을 따라야 합니다:



저작자표시. 귀하는 원저작자를 표시하여야 합니다.



비영리. 귀하는 이 저작물을 영리 목적으로 이용할 수 없습니다.



변경금지. 귀하는 이 저작물을 개작, 변형 또는 가공할 수 없습니다.

- 귀하는, 이 저작물의 재이용이나 배포의 경우, 이 저작물에 적용된 이용허락조건을 명확하게 나타내어야 합니다.
- 저작권자로부터 별도의 허가를 받으면 이러한 조건들은 적용되지 않습니다.

저작권법에 따른 이용자의 권리는 위의 내용에 의하여 영향을 받지 않습니다.

이것은 [이용허락규약\(Legal Code\)](#)을 이해하기 쉽게 요약한 것입니다.

[Disclaimer](#)

Master's Thesis of College of Agriculture and Life
Science

Development of an automated ground-
based hyperspectral field spectroscopy
system that integrates two geometric
observation configurations

두 개의 기하학적 관찰 구성을 통합하는 자동화된 지상
기반 초 분광 시스템 개발

August 2022

Graduate School of College of Agriculture and Life
Sciences

Seoul National University

Interdisciplinary Program in Agricultural and Forest
Meteorology Major

Jeongho Lee

Development of an automated ground-
based hyperspectral field spectroscopy
system that integrates two geometric
observation configurations

PROFESSOR Youngryel Ryu, Ph.D.

Submitting a Master's Thesis to the
College of Agriculture and Life Sciences

August 2022

Graduate School of College of Agriculture and Life
Sciences

Seoul National University

Interdisciplinary Program in Agricultural and Forest
Meteorology Major

Jeongho Lee

Confirming the Master's Thesis written by
Jeongho Lee

August 2022

Chair Kwangsoo Kim (Seal)

Vice Chair Youngryel Ryu (Seal)

Examiner Hyunseok Kim (Seal)

Abstract

Hyperspectral remote sensing is becoming a powerful tool for monitoring vegetation structure and functions. Especially, Sun-Induced chlorophyll fluorescence (SIF) and canopy reflectance monitoring have been widely used to understand physiological and structural changes in plants, and field spectroscopy has become established as an important technique for providing high spectral-, temporal resolution in-situ data as well as providing a means of scaling-up measurements from small areas to large areas. Recently, several tower-based remote sensing systems have been developed. However, in-situ studies have only monitored either BRF or BHR and there is still a lack of understanding of the geometric and optical differences in remote sensing observations, particularly between hemispheric-conical and bi-hemispheric configurations.

Here, we developed an automated ground-based field spectroscopy system measuring far-red SIF and canopy hyperspectral reflectance (400-900 nm) with hemispherical-conical as well as bi-hemispherical configuration. To measure both bi-hemispherical and hemispherical-conical reflectance, we adopted a rotating prism by using a servo motor to face three types of ports that measure incoming-, outgoing irradiance and outgoing radiance. A white diffuse glass and collimating lens were used to measure the irradiance, and a collimating lens was used to measure the radiance with a field of view of 20 degrees. Additionally, we developed data management protocol that includes radiometric-, and wavelength calibrations. Finally, we report how BRF and BHR data differ in this system and investigated SIF and vegetation index from both hemispherical-conical and bi-hemispherical observation configurations for their ability to track GPP in the growing seasons of a deciduous broad-leaved forests

Keywords: *Field spectroscopy, Sun-Induced Chlorophyll fluorescence (SIF), Hyperspectral reflectance, Canopy structure, Reflectance factor*

Student Number: 2020-28835

Table of Contents

Abstract	i
Chapter 1. Introduction	1
1.1. Study Background	1
1.2. Purpose of Research	4
Chapter 2. Developing and Testing of Hyperspectral System	6
2.1 Development of Hyperspectral System and Data Collecting	6
2.1.1 The Central Control Unit and Spectrometer	6
2.1.2 RotaPrism	8
2.1.3 Data Collection	10
2.3 Data Managing and Processing	12
2.3.1 Preprocessing of Spectra	12
2.3.2 Radiometric Calibration	14
2.3.3 Retrieval of SIF and Vegetation Indices	16
2.4 Ancillary Measurements to Monitoring Ecosystem.	18
Chapter 3. Application of Hyperspectral System	20
3.1 Study Site	20
3.2 Diurnal and Variation of Spectral Reflectance and SIF ..	21
3.3 Seasonal Variation of Vegetation Index and SIF	23
3.4 Broader Implications	25
Chapter 4. Summary and Conclusions	27
Bibliography	29

Chapter 1. Introduction

1.1. Study Background

Hyperspectral remote sensing is becoming a powerful tool for monitoring vegetation structure and function. Past studies on vegetation functions, the biochemical mechanisms of photosynthetic enzymes (Kubelka and Munk, 1931, McAlister and Myers, 1940), and the relationship between photosynthetic processes and environmental variables (Gabrielsen, 1949, Billings, Clebsch, et al., 1961, Björkman and Holmgren, 1963, Björkman, 1966, Schulze, 1966) fundamentally advanced the understanding of leaf photosynthesis. The structure of pigments directly impacts the spectral properties of the leaf. The study of leaf spectral properties, allowed the linking of remote sensing to photosynthesis (Sims and Gamon, 2002, Gitelson, Keydan, et al., 2006, Feret, François, et al., 2008). With this progress, the PROSPECT model (Jacquemoud and Baret, 1990) was developed as a radiative transport model based on Allen's generalized plate model (Allen and Richardson, 1968) that represents the optical properties of plant leaves from 400 nm to 2500 nm. The PROSPECT model was developed into PROSPECT-D (Féret, Gitelson, et al., 2017), which simulates anthocyanins, chlorophylls, and carotenoid dynamics. Fluspect-B (Vilfan, Van der Tol et al., 2016) simulates chlorophyll fluorescence for a given emission efficiency and a given spectral shape of chlorophyll for PS-I and PS-II emissions. The modeling of photosynthesis from leaf to canopy was also achieved. The AGR model of Allen, Gayle, and Richardson (Allen, Gayle, et al., 1970) is an extension of the Kubelka-Munk (Kubelka and Munk, 1931) theory of light scattering and extinction in diffusing media. The Suits model (Suits, 1971) and SAIL model (Verhoef, 1984) were developed by extending the AGR model, the concept of the spectral characters, and viewing-geometric effects. These advances provided the opportunity to calculate the directional reflectance as a function of the

measurement conditions and the canopy parameters. These achievements made remote sensing important in monitoring vegetation structure and function.

The evolution of SIF research has made hyperspectral remote sensing a more powerful tool. Unlike the other vegetation indices, SIF is linked directly to photosynthesis as light is intercepted by chlorophyll in leaves. This step forward allows for advanced photosynthesis research in natural environments, which is unprecedented. Wider SIF monitoring has been used to understand plants' physiological and structural changes. While SIF has an intrinsic, underlying relationship with canopy light capturing and light use efficiency, these physiological relationships are obscured by the fact that satellites can only observe a small and variable fraction of the total canopy SIF. For this reason, applying the LUE framework ($\text{Observed SIF} = \text{APAR} \times \text{SIF yield} \times \text{escape ratio}$) is useful approach to link SIF and canopy photosynthesis. However, many studies suggest that SIF may not be the optimal index. A case in point is Ben's NIRvP, which investigated the relationships between SIF and variables that at least partly capture the canopy structure component of SIF. The findings indicate that the contribution of leaf physiology to IF variability is small compared to the structural and radiative components. Stimulated by the development of the 8th Earth Explorer satellite mission, the Fluorescence Explorer (FLEX) by the European Space Agency (ESA), and the advanced exploitation of atmospheric missions, like Sentinel-5P, GOSAT, and OCO-2, researchers across the globe greatly advanced the field of fluorescence spectroscopy over the last decade, resulting in versatile instrumentation and approaches to retrieve SIF. Despite these efforts, uncertainties about SIF magnitude are still unresolved.

Field spectroscopy underpins the development of long-term imaging spectroscopy, but the two techniques have many things in common as they aim to obtain accurate data on the spectral reflectance of Earth's surface from a distance. Since field spectroradiometers were first used to study human color vision,

particularly and later the color of the Earth's surface from the air (Penndorf, 1956), field spectroscopy has played various roles in remote sensing. The first is a cross-validation role for in situ point spectroscopy and airborne imaging spectroscopy data and to quantify sources of uncertainties that can affect such validations. The large viewing angles of many satellite products, e.g., MODIS, result in inaccurate and variable footprint areas leading to additional geometric uncertainty (Tan, Woodcock, et al., 2006). In addition, air and space-borne data needs to be corrected for atmospheric absorption and scattering effects, which can add to uncertainty (Drolet, Huemmrich, et al., 2005, Hilker, Lyapustin, et al., 2009). Second, field spectroscopy is considered a solution for advanced point observations at the landscape and earth level when applying Eddy Covariance technology at the ecosystem level. Effective integration of flux measurements across scales through optical remote sensing is essential to understand the global pattern of the surface-atmospheric fluxes of carbon and water vapor. However, the footprint mismatch between Eddy Covariance observations and data derived from much coarser satellites complicate the integration of the two data sources. These physical limitations could be significantly reduced by in situ long-term spectral measurements, which are less technically difficult, as sensing devices could be held over the target area for much longer, and the path length between the instrument and the target area for measurement is reduced.

There are two widely used categories of viewing geometry for tower-based hyperspectral systems collecting canopy reflected radiance: hemispherical-conical and bi-hemispherical observations. It is important to determine whether the bi-hemispherical or hemispherical-conical systems should be used, and that determination is dependent on the research objectives. The bi-hemispherical system, whose SIF signal is from a large footprint, should be used when the objective is to complement eddy flux observations for ecosystem process studies (Gu, Wood, et al., 2019). In contrast, the hemispherical-conical system, which has a much smaller footprint, may offer better potential if the objective is

to validate satellite measurements. Different system configurations (i.e., bi-hemispherical vs. hemispherical-conical). The retrieval methods can bias the SIF magnitude and distort the diurnal shape, therefore confounding the interpretation of inherent strength and dynamics of SIF emission. The differences in the measured SIF between the bi-hemispherical and hemispherical-conical systems can be theoretically reconciled through advances in retrieval methods and improved SIF radiative transfer modeling. Critically, the difference in the FOV between hemispherical-conical and bi-hemispherical systems affect the diurnal cycle of the observed reflectance and the relationship between SIF and GPP. However, despite its importance, the differences between the two types of field observation instrument configurations, regarding the portion of reflectance observed in their FOV and their temporal covariation with canopy photosynthesis, are yet to be characterized. An in-depth understanding of the contribution of reflectance to SIF diurnal dynamics from hemispherical-conical and bi-hemispheric observation configurations would improve GPP modeling accuracy using SIF measurements. Despite this, there has not been much research on different system configurations (i.e., bi-hemispherical vs. hemispherical-conical) and retrieval methods.

1.2. Purpose of Research

To address this, an automated ground-based hyperspectral field spectroscopy system that integrates two geometric observation configurations and a data quality management protocol for measuring far-red SIF and canopy reflectance (400–900 nm) was developed. The measurements by this system allow for the calculation of vegetation indices, such as the normalized difference vegetation index (NDVI), the enhanced vegetation index (EVI), the near-infrared radiance of vegetation (NIRv), and the photochemical reflectance index (PRI). First, a system enclosure to control temperature and humidity for hyperspectral radiometer stability was designed. The enclosure also provided power and a network

connection via the Internet. Second, to measure bi-hemispherical and hemispherical-conical reflectance, a RotaPrism, a rotating prism using a servo motor to measure upward- and downward-facing irradiance and outgoing radiance, was modified. Third, a quality control protocol to remove outliers and fill data gaps with machine learning algorithms were developed. Finally, the performance of the data quality protocol and the results of the diurnal and seasonal patterns of deciduous forests were shown.

Chapter 2. Developing and Testing of Hyperspectral System

2.1 Development of Hyperspectral System and Data Collecting

2.1.1 The Central Control Unit and Spectrometer

The theoretical significance of misunderstandings caused by differences in bi-hemispherical and hemispherical-conical measurements led to the development of a novel ground-based hyperspectral system to spatially resolve far-red SIF and vegetation index observations simultaneously as well as addressing reflectance measurement issues. The system consists of two parts: a system enclosure for stable data collection and a RotaPrism that enables simultaneous bi-hemispherical and hemispherical-conical measurements (Figure 1).

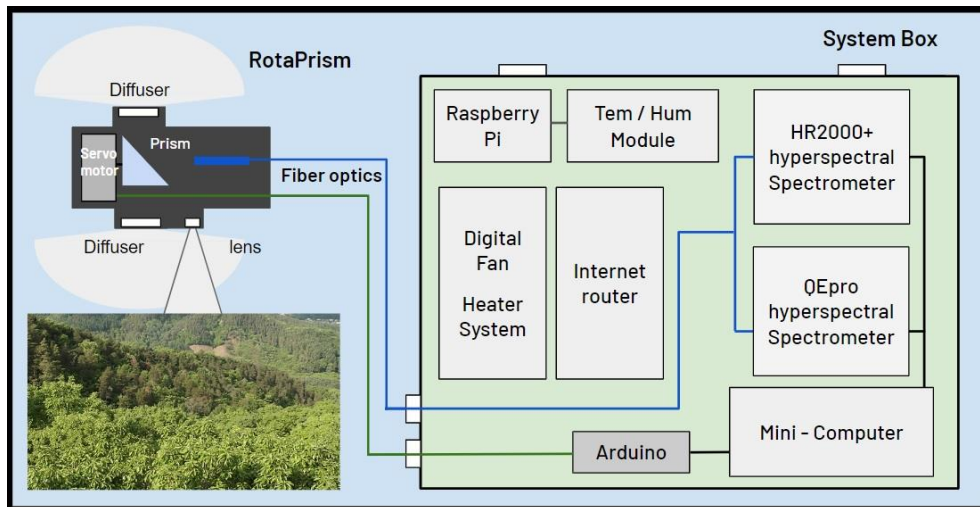


Figure 1. Overview of a hyperspectral system

The system was designed with an enclosure to control the temperature and humidity for hyperspectral radiometer stability. It also provided sufficient power and a network connection via the Internet. Spectroradiometers are enclosed in the system enclosure and have a temperature-controlled function at 25 ° C. To record reliable data over a long period, the spectrometer must be kept at a

stable temperature, ensuring that the thermal noise level behaves predictably. Missing data should also be minimized due to the reliable electricity supply and the network connection via the Internet. The system hardware core consists of a Mini PC (PN51-S1, Asus Inc., FL, USA) as the central control unit, and two high-resolution, high-sensitivity spectrometers for measuring SIF and VNIR range reflectance (QE Pro, HR2000+, Ocean Optics Inc., Dunedin, FL, USA). Application software was developed using Omni Driver (Ocean Insight) development kits to facilitate automatic data collection by Java in the lab. Typically, spectrometers are controlled via application software.

The specific QE Pro spectrometer used in the system has a typical SNR of 1,000 for a single integration period. It is equipped with a long pass filter (>695 nm), a $25\text{-}\mu\text{m}$ slit, and an H15 grating, resulting in a spectral range of 730-786 nm with a resolution of 0.15-0.17 nm. This spectral range is suitable for retrieving SIF at the O_2 A-band. Different fixed integration times between upward-facing (0.5 s) and downward-facing measurements (3.5 s) were used. The integration time value, when photosynthetically active radiation (PAR) peaks, was selected to avoid saturation in QE Pro data. The temperature of the thermoelectric cooler (TEC) of the QE Pro spectroradiometer was set at -20°C , and it was confirmed that there was a relatively small variation in actual TEC temperature during the measurement period ($-18.0 \pm 1.29^\circ\text{C}$). It is equipped with a long pass filter (>695 nm), a $25\text{-}\mu\text{m}$ slit, and an H15 grating, resulting in a spectral range of 350-1050 nm with a resolution of 0.15-0.17 nm. These two spectrometers are linked by bifurcated fibers providing 1:2 routing in a Y-configuration. The two fibers are bundled at one end, branching into separate “legs.” This allows fibers of the same or different core diameters or wavelength ranges to be used in each leg. A fiberoptic cable is used to measure photons from targets using the RotaPrism (i.e., outgoing irradiance and radiance from vegetation and incoming solar irradiance) to the spectrometer.

2.1.2 RotaPrism

A custom-made rotating prism system was developed using a RotaPrism for collecting spectral data with spectroradiometers. Figure 2 shows the mechanical details of the RotaPrism that samples the incoming irradiance, radiance, and irradiance reflected from the forest canopy. The RotaPrism consisted of a microcontroller (Arduino Nano; Arduino, NY, USA) that controls a servomotor (HS311; HITEC, Seoul, South Korea), two 12.5-mm aluminum and MgF₂-coated N-BK7 right angle prisms (Edmund Optics, Barrington, NJ, USA), two white diffuse glasses (Edmund Optics), two achromatic collimating lenses (74-ACR; Ocean Insight), and a 600- μ m core fiber optic cable (Ocean Insight). The main prism is mounted on a rotating optical assembly and is turned by a servomotor mounted in the RotaPrism below. A 600- μ m-diameter silicon optical fiber is connected to the front and is located on the optical axis of the prism system to allow for the collection of light that will be transmitted to the spectrometer.

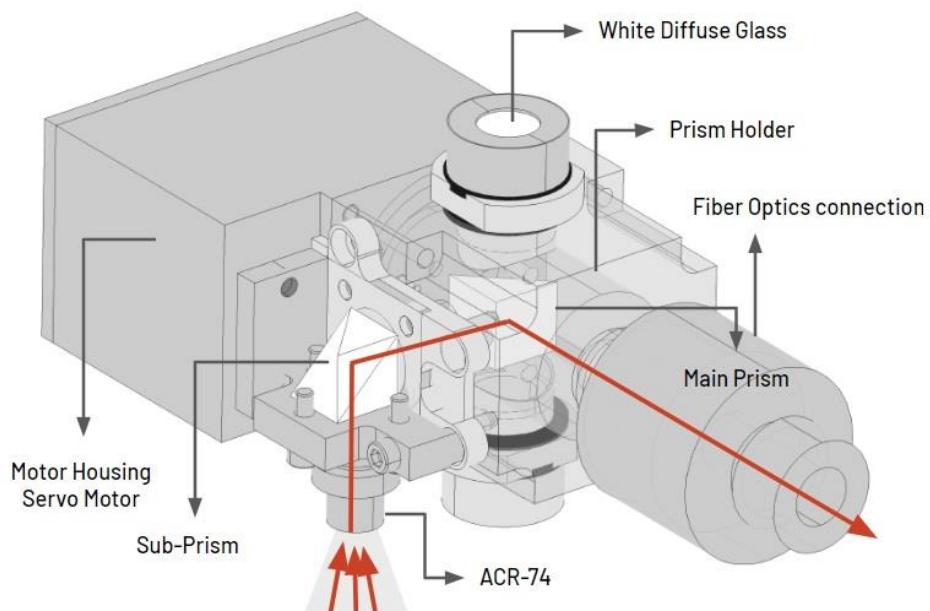


Figure 2. Overview of the RotaPrism and the prism position for each measurement mode, Radiance mode light path is depicted as the red line. The main prism and prism holder are controlled using a

servomotor to adjust the measurement mode.

On either side of the RotaPrism is a cosine-corrected hemispherical diffuser to sample the incoming and outgoing irradiance. Below the diffuser, a prism is mounted on a holder. The holder is mounted on a small translation stage, and the position of the stage determines where radiation is sampled; the sky or the canopy. The translation stage is driven by a small servomotor that rotates the prism between four fixed angles, corresponding to incoming irradiance, outgoing irradiance, outgoing radiance, and dark current measurements; each end of the translation stage has a buffer time of 5 s to avoid the overlap of signals (Figure 2). The RotaPrism performs four functions:

1. The dark current is measured by blocking all external light. The dark current is subtracted from the other signals before processing. In this case, the main prism orientation is towards the holder, which blocks the sampling port. The RotaPrism housing excludes light as it is painted black. It also excludes light using a layer of black felt attached to the underside. There are three main reasons to subtract the dark measurement: first, it removes the baseline from other measurements; second, it removes the dark current contribution from the measurement; and third, it can be used to eliminate any background light.

2. It measures the irradiance incident on the canopy or the irradiance reflected by a cosine-corrected hemispherical diffuser. If the main prism orientation is towards the upward (0°) or downward (180°), the prism holder ensures light passes through the diffuser and is sampled by the optical fiber for eventual transmission to the spectrometer.

3. It measures the radiances reflected on the canopy via a sub-prism and a collimating lens. The main prism is positioned so that the diffuser port is blocked, and light from the target is

reflected onto the optical fiber field-of-view (FOV). The main-prism orientation is oriented at 45° at that time. The incidental light from the target is collected by the collimating lens with a 20° field of view and is reflected through the sub-prism to the main prism. The field-of-view of radiance measurement was set to 20° by adjusting the focal length in a darkroom (Figure 3).

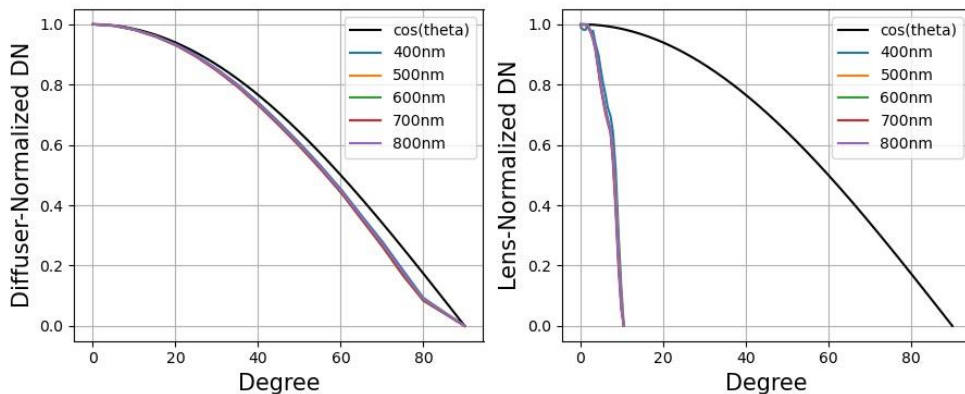


Figure 3. Field-of-view test of radiance and irradiance port. The radiance port FOV was set to 20° by adjusting the focal length in the darkroom. Through in the above test, it was confirmed that the irradiance port follows the cosine response function well.

2.1.3 Data Collection

Far-red SIF (760 nm) and spectral reflectance (400-900 nm) were measured using QE Pro and HR2000+ spectroradiometers (Ocean Insight, Dunedin, FL, USA) and RotaPrism installed at the top of the 40 m tower (approximately 20 m above the canopy). Data was recorded between 05:30 and 20:30 continuously at 1-minute intervals. In the data collection sequence, the single beam sandwich method was employed to collect the down-welling and up-welling spectra, following the method proposed by previous works (Cogliati, Rossini, et al., 2015). The schematic observation sequence is displayed in Figure 4. The first and second down-welling solar irradiance and up-welling

irradiance are sequentially collected by controlling the RotaPrism. The effect of the variation in solar irradiance resulting from a time delay can be reduced by averaging the two down-facing irradiance measurements. Under normal conditions, an entire measurement can be accomplished within 1 min. The dark currents (DC) resulting from the thermal and readout noise vary based on the integration time and the temperature. Thus, the DCs is recorded at the end of each measurement sequence.

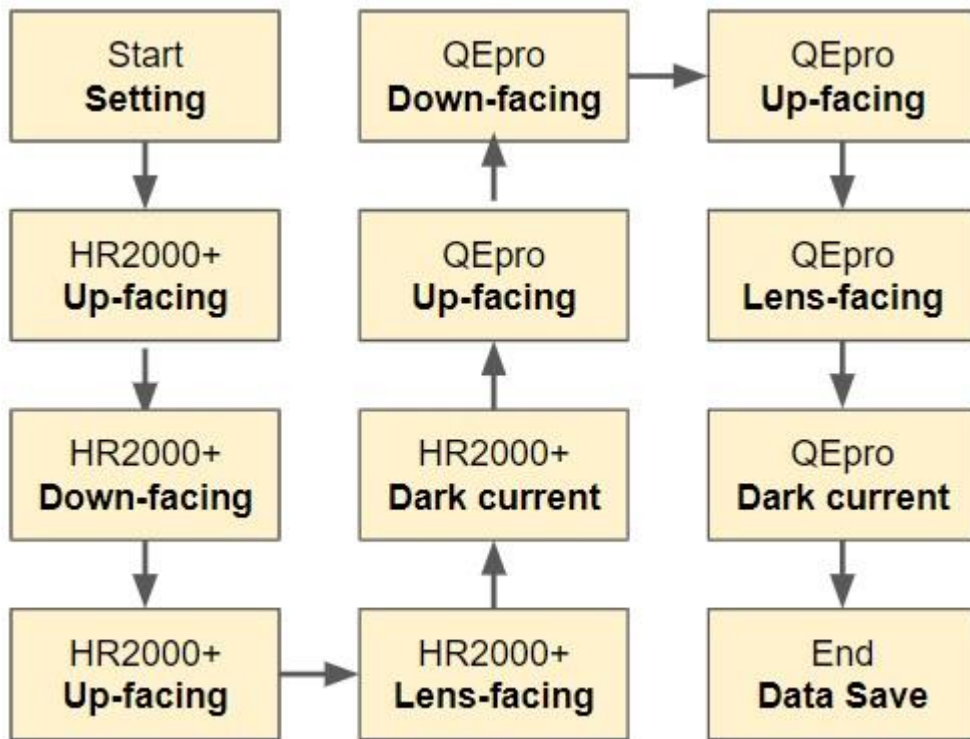


Figure 4. Schematic observation sequence

2.3 Data Managing and Processing

2.3.1 Preprocessing of Spectra

Acquired field spectroscopy data progress typically through processing levels from raw data to derived products (Chisholm, Hueni, et al. 2015) (Figure. 4). According to the information theory, the higher the processing level, the more meaningful the data (Floridi, 2005, Rowley, 2007), and, consequently, the higher the number of potential users. The tower data processing differed for each site because the researcher managing each site differed. A common protocol for managing and processing field site data is essential. In addition, by dividing the data level, the quality of each level of data can be controlled. Furthermore, in situ spectral data is often used to validate airborne and satellite data and is commonly referred to as ground truth. The processing levels of airborne imaging and ground-based non-imaging spectrometers are identical. Thus, separating the data levels forms effective data management and recognizes the importance of data quality and the difficulties associated with cross-validation strategies of field and airborne spectroscopy data at various processing levels within the spectral information hierarchy.

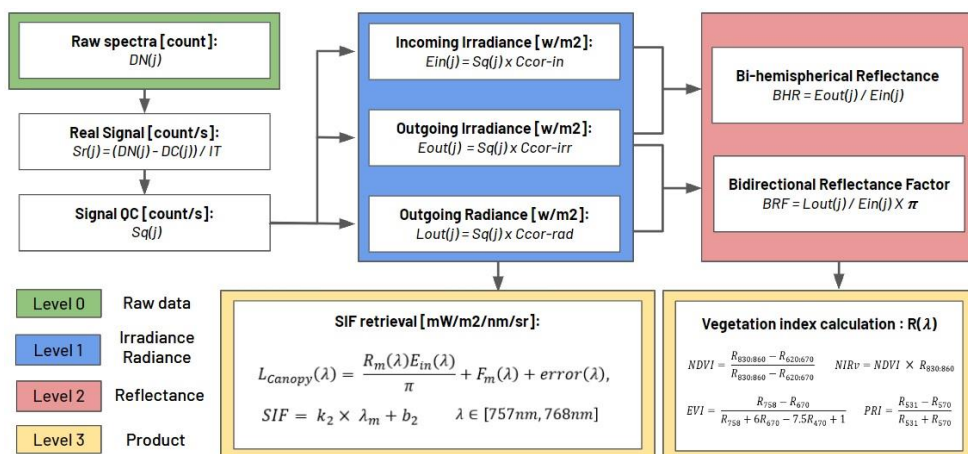


Figure 4. Data Managing and Processing Protocol

Level 0 holds raw digital numbers (DN), and sensor-generated files, stored as binary objects on a file system. Level 1 refers to spectral measurements, such as radiance and irradiance traceable on an international standard, in other words, radiometrically calibrated data. Level 2 comprises reflectance factors of a hemispherical-conical or bi-hemispherical beam geometry, which may differ depending on the instrument setup, the irradiance/radiance, reflectance factors, and conversion algorithms. Level 3 incorporates derived biogeophysical information, for example, estimated vegetation properties.

The measurement value (DN, Level 0) generally has 3 contributions: the signal (S) caused by light. The dark current (DC), as was discussed above, and the baseline (BL) for each wavelength, λ , can be determined using Equation (1):

$$DN(\lambda) = S(\lambda) + DC(\lambda) + BL(\lambda) \quad (Eq.1)$$

The real signal (S_r) originating from electrons absorbing one photon rises linearly with integration time (IT). As described above, when measuring using the RotaPrism, the BL value is included in the DC value as DC is directly measured. Accordingly, the real signal is calculated using Equation (2):

$$S_r(\lambda) = \frac{DN(\lambda) - DC(\lambda)}{IT} \quad (Eq.2)$$

Eq. 2 is applied to up-facing (DN_{up}), down-facing (DN_{dw}), and lens-facing (DN_{rad}) DNs, and it calculates radiance incoming irradiance (E_{in}), outgoing irradiance (E_{out}), and outgoing radiance (L_{out}), (Level 1) through each radiometric coefficient (C_{cal}). The following section describes the radiometric calibration process and coefficient calculation in detail. The reflectance factor (Level 2), R , is defined as the ratio of the radiant flux reflected by a surface that is reflected into the same beam geometry and wavelength range as an ideal and diffuse (Lambertian) surface irradiated under the same conditions. Based on the concepts, corresponding mathematical

formulas can be derived for the most relevant quantities used in remote sensing, namely HCRF (Hemispherical–Conical Reflectance Factor: surface reflectance) and BHR (Bi–hemispherical Reflectance: Albedo). The basic retrieval scheme starts with hemispherical–conical observations. Most existing processing approaches assume that the HDRF is constant over the full cone angle of the instrument (IFOV). Thus, the HCRF numerically equals the HDRF without correction (Equation (3)). The algorithm for retrieving the HCRF and BHR from MISR top–of–atmosphere (TOA) radiances is virtually independent of the surface, and the BRF model and its accuracy depends on the accuracy of the atmospheric information (Martonchik et al., 1998). Assuming that the atmospheric conditions are constant, the BRF algorithm can be replaced by multiplying π . Calculating the reflectance factor is done using the following (Equation (4)):

$$HCRF = \frac{L_{out}}{E_{in}}, \quad HCRF \approx HDRF \quad (Eq.3)$$

$$BRF = HDRF \cdot \pi, \quad BHR = \frac{E_{out}}{E_{in}} \quad (Eq.4)$$

BRF and BHR are used to calculate derived products, such as biogeophysical information. High–level products are described in the following section.

2.3.2 Radiometric Calibration

The complex environments experienced during long–term unattended field measurements degrade the performance of spectrometers, optical fibers, and the RotaPrism. Therefore, regular calibrations must be performed to maintain the quality of the observed spectra, especially for SIF retrieval. This is particularly relevant for the narrow absorption band's precise location and absolute irradiance. The complex field installation and optical setup require that radiometric calibration of the system be conducted in

the field. This is often done on top of a tower above the canopy (Figure 5).



Figure 5. Radiometric calibration is conducted in the field, often on top of a tower above the canopy.

The calibration is determined for each spectrometer, i , by relating the measured signal $S_r(\lambda)$ (units: counts/s) to the irradiance $E(\lambda)$, radiance $L(\lambda)$ with a calibration factor, $C_{cal-irr}(\lambda)$, $C_{cal-rad}(\lambda)$. Calculating the calibration factor is done using the following Equation (5):

$$E(\lambda) = C_{cal-irr} \cdot S_r(\lambda), \quad L(\lambda) = C_{cal-rad} \cdot S_r(\lambda) \quad (Eq. 5)$$

For the determination of $C_{cal}(\lambda)$, a calibrated diffuse reflectance standard (4-inch integrating sphere, LabSphere Inc., NH, USA) is mounted below and in front of the RotaPrism port assembly. This integrating sphere is highly Lambertian and has a reflectivity of over 99%. The RotaPrism is pointed at the reflectance standard, and measurements of the reflected flux of the standard light source (SCL-050, LabSphere Inc., NH, USA) are performed continuously with an integration time of 2-6 s.

Several strategies are applied to ensure high-quality radiometric calibration. First, an integrating sphere customized for the RotaPrism is used to calibrate the HR2000+ and QE Pro at monthly intervals. When using a light source, both the light source and the cosine corrector are shielded from direct sunlight to avoid stray light effects. Second, the QE Pro and HR2000+ data was compared to confirm that consistent radiometric calibration. The radiometric irradiance data within the overlapping spectral region (730-780 nm) of the two spectrometers was consistent over the entire measurement period (Figure 6) ($R2 > 0.98$). The wavelength calibration was also performed using a calibration light source (HG-1; Ocean Insight).

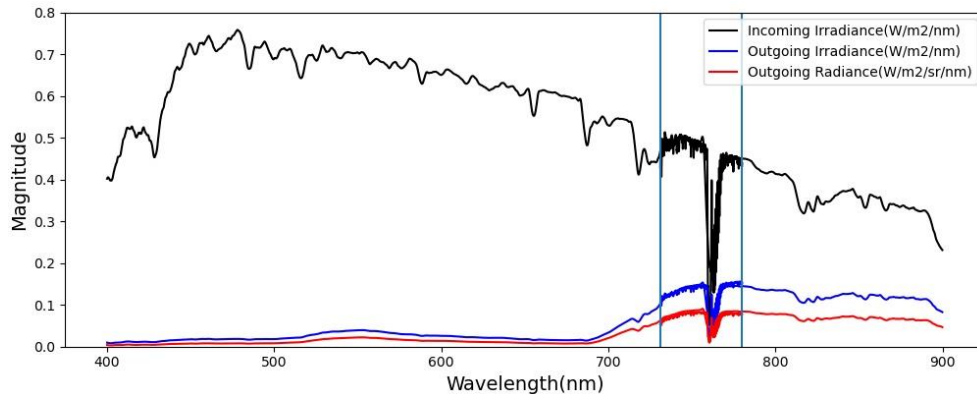


Figure 6. Example of single spectral data acquisition over a vegetated surface. Down- and up-welling irradiances and radiance for the HR2000+ and QEpro spectrometers. The bold line is spectral data from QEpro.

2.3.3 Retrieval of SIF and Vegetation Indices

The spectral fitting method, SFM (Mazzoni, Meroni, et al., 2012) for SIF retrievals, was used. SFM assumes that the spectral changes in reflectance (R) and SIF (F) at selected spectral intervals can be described as polynomials of wavelength (λ) or other suitable mathematical functions. The SFM assumed that both R and F are linearly related to λ . Therefore, the measured canopy

radiance ($L_s(\lambda)$) can be expressed as Equation (6):

$$L_{Canopy}(\lambda) = \frac{R_m(\lambda)E_{in}(\lambda)}{\pi} + F_m(\lambda) + error(\lambda), \quad \lambda \in [\lambda_1, \lambda_2] \quad (Eq.6)$$

where $R_m(\lambda) = k_1 \times \lambda + b_1$ and $R_m(\lambda) = k_2 \times \lambda + b_2$ are the linear functions. k_1 , b_1 , k_2 , and b_2 are the coefficients of the linear functions describing R , and F . $E(\lambda)$ is the measured incident solar irradiance, calculated as the mean value of E_{g1} and E_{g2} . $error(\lambda)$, the modeling error of observed and simulated radiance. λ_1 and λ_2 were set as 757 and 768 nm, respectively. Far-red SIF was focused upon; red SIF certainly deserves further investigation, as it is a signal complicated by canopy re-absorption (Chang et al., 2020). SIF was quantified as a linear function of wavelength λ_m and can be calculated using the following Equation (7):

$$SIF = k_2 \times \lambda_m + b_2 \quad (Eq.7)$$

where λ_m is the wavelength at which incident solar irradiance reached the minimum value within the broader O_2 absorption band around 760 nm.

Vegetation indices to assess greenness, chlorophyll content, or leaf area index, are determined based on the differences in the surface reflectance between the blue, red, and near-infrared wavelength region of the spectra (LAI) (Porcar-Castell, Tyystjärvi, et al., 2014). The spectra of the HR2000+ are used to calculate the average reflectance $R(\lambda)$ at a specific wavelength λ or a wavelength range $\lambda_1 - \lambda_2$, where the four vegetation indices are routinely retrieved. The measure of the greenness of the canopy is referred to as the Normalized Difference Vegetation Index (NDVI) ((Tucker, 1979, Carlson and Ripley, 1997, Rascher, Alonso, et al., 2015). The greenness observation is supplemented by the Enhanced Vegetation Index (EVI) as it corrects for structural and atmospheric effects through the differential weighing of spectral regions and by considering an additional blue wavelength band (Huete, Liu, et al., 1997). By using the reflectance at 531 nm together with a reference band at 570 nm (Gamon, Penuelas, et

al., 1992), (Equations (7)–(10)), and the Photochemical Reflectance Index (PRI) has been used to estimate dynamics in the xanthophyll pigment interconversion (Magney, Vierling, et al., 2016).

$$NDVI = \frac{R_{830:860} - R_{620:670}}{R_{830:860} + R_{620:670}}, \quad NIRv = NDVI \times R_{830:860},$$

$$EVI = \frac{R_{758} - R_{670}}{R_{758} + 6R_{670} - 7.5R_{470} + 1}, \quad PRI = \frac{R_{531} - R_{570}}{R_{531} + R_{570}} \quad (Eq. 7\sim 10)$$

As the system records full spectra from 400 to 850 nm, it is possible to consider full spectral shapes beyond traditional vegetation indices, or general spectral decomposition, by using partial least squares (Serbin, Dillaway, et al., 2012) or other mathematical tools such as singular value decomposition (SVD).

2.4 Ancillary Measurements to Monitoring Ecosystem.

GPP was estimated by measuring the CO₂ flux above the canopy using an eddy covariance (EC) system. A three-dimensional sonic anemometer (CSAT-3; Campbell Science, Logan, UT, USA) and an open-path infrared gas analyzer (LI-7500A; LICOR, Lincoln, NE, USA) were installed at the height of 1 m on top of the 40 m tower, and data was processed using the 10-step KoFlux standardized data processing protocol (Kang, Kim, et al., 2018). A variety of corrections were used to convert raw data into high-quality flux data, including planar fit tilt correction (Wilczak, Oncley, et al., 2001), density fluctuation compensation (Webb, Pearman, et al., 1980), and frequency response correction (Horst and Lenschow, 2009, Fratini, Ibrom, et al., 2012); all corrections were applied using LICOR EddyPro software. Data quality control procedures, included removing outliers, filling data gaps using a marginal distribution sampling method (Reichstein, Falge, et al., 2005), and applying nighttime CO₂ flux corrections were performed using MATLAB (MathWorks Inc., Natick, MA, USA). After quality

control, 34.5% and 42.2% of CO₂ flux data was retained. Friction velocity (u^*) filtering (FVF; (Gu, Falge, et al., 2005, Reichstein, Falge, et al., 2005) and van Gorsel filtering (VGF) (Van Gorsel, Leuning, et al., 2007, van Gorsel, Leuning, et al., 2008, van Gorsel, Delpierre, et al., 2009) were used to correct CO₂ flux in estimates of GPP and ecosystem respiration (RE). These methods mitigate the effects of nighttime advection in mountainous terrain. Environmental and meteorological data were continuously collected and processed every half hour, including air temperature (Ta, HMP155, Vaisala Group, Helsinki, Finland), relative humidity (RH, HMP155, Vaisala Group, Helsinki, Finland), and total incident PAR above the canopy (PAR, LI-190SL, LI-COR Inc., Lincoln, NE, USA).

Chapter 3. Application of Hyperspectral System

3.1 Study Site

The measurement campaign was conducted in a deciduous forest in Gwangneung (Pocheon-si, Gyeonggi-do, Republic of Korea; Figure 7) during the growing season when the variation of the canopy structure is large. The average annual temperature at the site is 11.5 ° C, and the average annual precipitation is 1332 mm. The regional climate is a typical temperate climate, with hot and humid summers due to the influence of the East Asian monsoon. and dry snowy winters. The hyperspectral system was located at the top of a 40m tower. The topography around this tower slopes down by about 10° to the east. Detailed information on this site has been previously published (Jong-Hwan, Joon, et al., 2003, Kim, Lee, et al., 2006, Kang, Park, et al., 2009).



Figure 7. The eddy covariance tower and surrounding forest at the study site.

3.2 Diurnal and Variation of Spectral Reflectance and SIF

Figure 8 shows the two reflectance factors: the BHR and the BRF. Although they differ in magnitude Fig. 8(a) and diurnal evolution Figs. 8(b) and 8(c), at wavelengths of 680 and 800 nm, respectively, show the vegetated surface's overall shape. A more comprehensive explanation of these differences can be attained by considering that BRF measurements are obtained by observing the canopy within a limited sightline, while BHR measurements receive contributions from all directions.

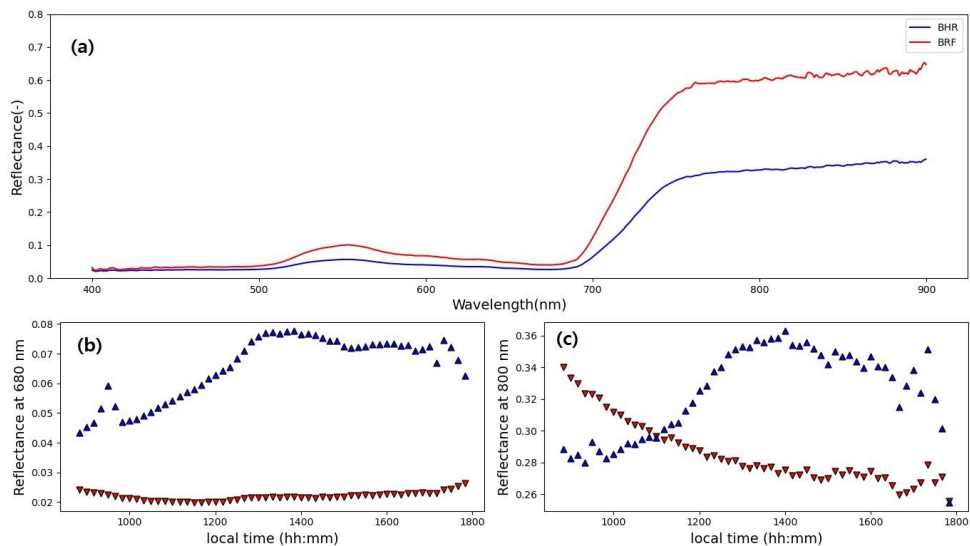


Figure 8. (a) Reflectance factors BHR and BRF measured at noon; (b) and (c) the diurnal evolution of BHR and BRF for wavelengths 680 and 800 nm, respectively. Measurements were collected under clear sky conditions on 05/15/2022.

The different geometries of the optics employed by the spectral systems cause the different diurnal evolutions of the two reflectance factors. In fact, when the Sun approaches its maximum

height, the canopy has an almost zenithal illumination; therefore, the BRF takes in significant contributions from the soil beneath the vegetation, but since that contribution depends on wavelength, it has a higher or lower reflectance than the vegetation. At wavelengths shorter than the red edge (roughly 700 nm), vegetation is normally darker than the nearby soil, while vegetation is generally brighter for wavelengths greater than 730 nm. The Sun elevation and the canopy structure have the effect of including or excluding soil contributions from BRF; for lower Sun altitudes, the soil is not directly illuminated. Based on this, it is expected that a convex or a concave curve, depending only on the selected wavelength, can represent the diurnal variation of the monochromatic BRF. The curve should be convex, with a maximum at noon for wavelengths shorter than 700 nm and concave for wavelengths longer than 730 nm. The above agrees with all results obtained in this study (Figure 9).

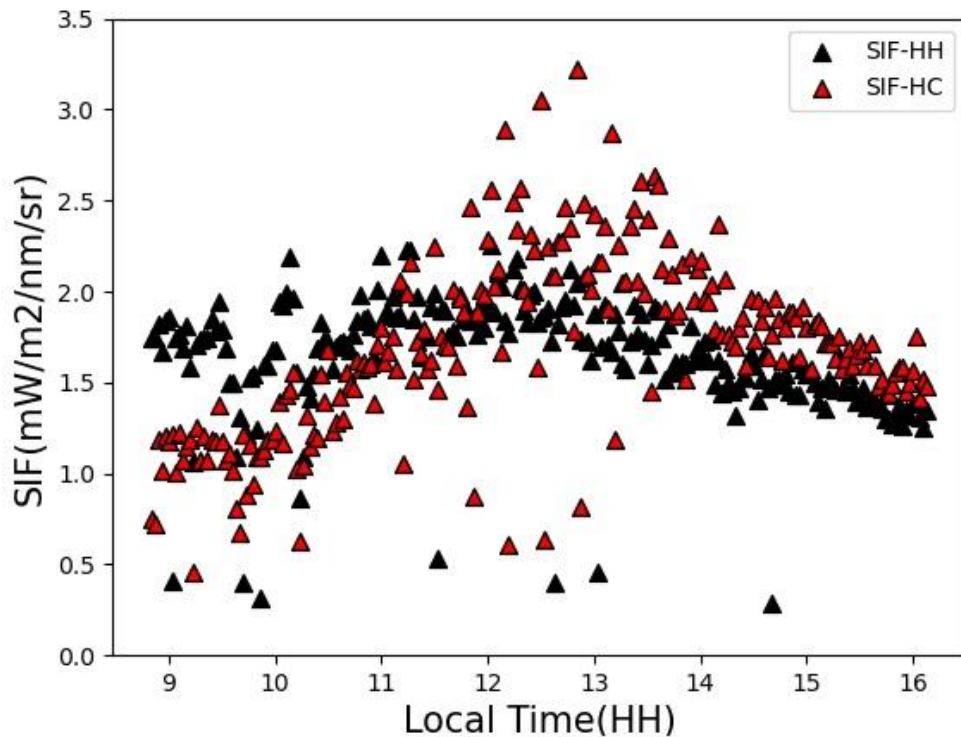


Figure 9. Diurnal variation of SIF. Measurements were collected

under clear sky conditions on 06/02/2022.

The BHR has a much more complex behavior because the soil contributions cover only a narrow sector of the hemispherical FOV, and the bidirectional reflectance distribution function (BRDF) hot-spot and secularity are always in the instrument FOV for any Sun elevation. These contributions likely have a slight impact on the BHR of natural targets, which aligns with the results of previous studies (Barducci, Guzzi, et al., 2009). For high Sun elevations, a large portion of the down-welling radiation is converted into heat as it penetrates the canopy and soil. Conversely, at large off-zenith illumination angles, a larger portion of the incoming light escapes the canopy and remains available for observation, resulting in a higher BHR. These mechanisms largely depend on the canopy geometry and structure and are therefore independent of wavelength, which aligns with the experimental results (Figures 8b and 8c). In accordance with the albedo trend reported in a previous study (Strub, Schaepman, et al., 2003), BHR shows an asymmetric behavior with albedo being higher in the morning than afternoon.

3.3 Seasonal Variation of Vegetation Index and SIF

Figure 11 shows the system products calculated from two different configurations: Bi-hemispherical and Hemispherical-Conical during the growing season. The SIF data was averaged into half-hour values after quality control. In order to explicitly present the seasonal variability of SIF in tandem, all variables were also processed into half-hour averages.

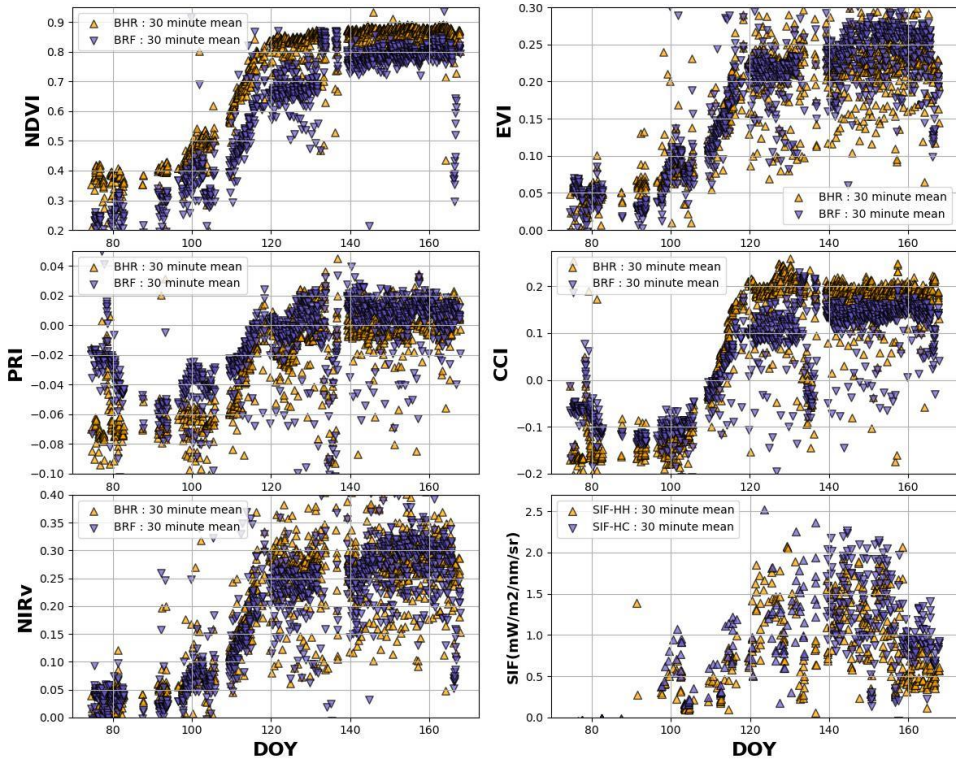


Figure 10. Seasonal variation of Vegetation Index and SIF of a) NDVI, b) EVI, c) PRI, d) CCI, e) NIRv, f) SIF of the growing season at Gwangneung deciduous forest (DOY 75–168)

The variation in NDVI and EVI are presented in Figures 10a and 10f, respectively. The NDVI is a good indicator of vegetation growth. EVI is similar to NDVI and can be applied to quantify vegetation greenness. Additionally, EVI corrects for atmospheric conditions and background noise due to the canopy and is, therefore, more sensitive in areas with dense vegetation. EVI decouples the canopy background signal and reduces atmosphere influences. This makes it an 'optimized' vegetation index that can enhance the sensitivity of vegetation signals in high biomass regions and improve vegetation monitoring. It was found that the NDVI and EVI slopes between DOY 100–140 are different due to the difference in canopy density (Figure 11).

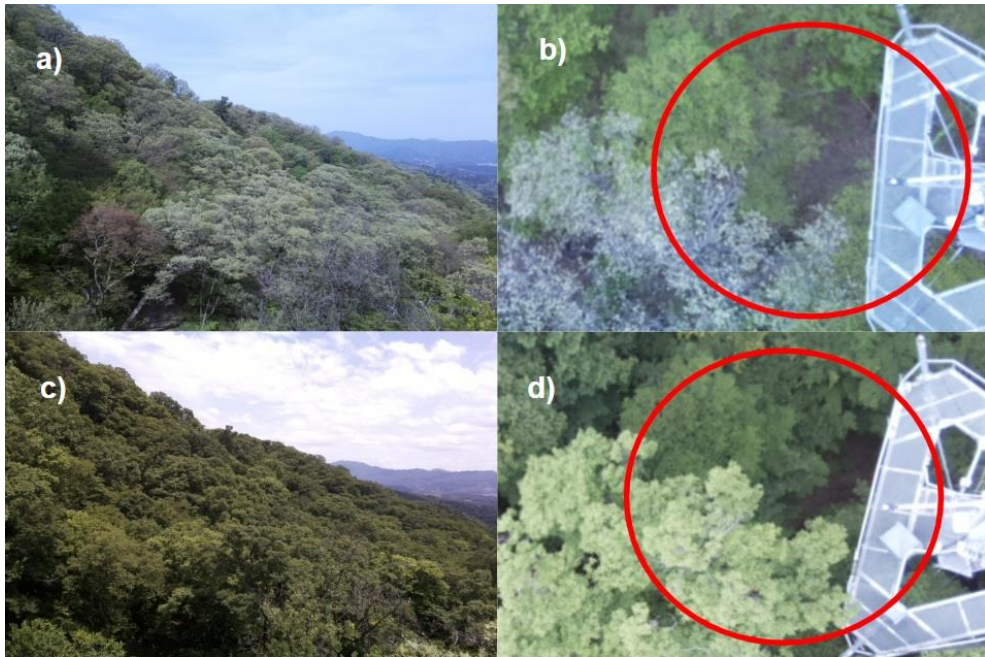


Figure 11. The footprint of the hyper-spectral system. a, c) BHR footprint (DOY 103, 168), b, d) BRF footprint (DOY 102, 168)

Overall, the seasonal dynamics of SIF values at both the O_2 -A and the O_2 -B bands are consistent with the variation in PRI. PRI is positively correlated with LUE through the entire season (Hall, Hilker, et al., 2008) (a few studies suggest that seasonal PRI is controlled partially by pigment pool size) (Wong and Gamon, 2015) and a positive relationship between SIF and PRI further supports the findings above. A positive correlation between SIF and PRI was also found for cropland systems (Middleton, Cheng, et al. 2009, Cheng, Middleton, et al., 2013). Future studies must extend to other biome types, including tropical forests and arctic tundra (Rocha and Shaver, 2011, Lee, Frankenberg, et al., 2013).

3.4 Broader Implications

The findings demonstrate that the instrument configuration can heavily influence the diurnal shape and the magnitude of retrieved SIF. Previous studies (Liu and Liu, 2018, Sabater, Vicent, et al., 2018) have identified a distortion effect caused by

atmospheric in-filling that affects the SIF retrieved from telluric oxygen bands. Naturally, bi-hemispherical systems will collect more diffuse radiation from a wider field using a cosine corrector and, therefore, would be more susceptible to such distortion effects. Another study (Zhang, Zhang, et al., 2019) compared several bi-hemispherical and hemispherical-conical systems. While their study did not discuss the impacts of diffuse radiation on SIF retrieval, they presented evidence that bi-hemispherical systems exhibit greater distortion around the edges of the oxygen bands than hemispherical-conical configured systems. To verify these points, the difference between two different geometric configuration observations can be analyzed by installing the developed hyper-spectral system in various biomes (for example, wetlands, crops, tropical forests, etc.).

It is important to decide whether the bi-hemispherical or hemispherical-conical systems should be used, depending on the research objectives. The bi-hemispherical system, whose SIF signal is from a large footprint, should be the choice when the objective is to complement eddy flux observations for ecosystem process studies (Gu, Wood, et al., 2019). In contrast, the hemispherical-conical system, which has a much smaller footprint, may be better if the objective is to validate satellite measurements. Therefore, the hyper-spectral system developed in this study utilizes simultaneous observation of geometric configuration to verify the above hypothesis at various sites (bi-hemispherical - GPP, hemispherical-conical - validating drone and satellite measurements). Theoretically, the differences in the measured SIF between the bi-hemispherical and hemispherical-conical systems can be reconciled through advancements in retrieval methods and SIF radiative transfer modeling. Such advances are greatly needed.

Chapter 4. Summary and Conclusions

An automated remote sensing system was developed for the simultaneous measurements of bi-hemispherical and hemispherical-conical configuration SIF and vegetation indices. The combination of bi-hemispherical and hemispherical-conical configuration SIF observations offers a unique opportunity. The development allows for the study of photosynthesis in a complex canopy. Information on SIF re-absorption in the red wavelength range in different layers of the canopy, as well as the responses to environmental stress factors, can be gathered.

The principle of the in-filling of solar Fraunhofer lines, also used for satellite SIF retrievals, and some ground-based SIF measurements enhance the instrument designed for highly stable and sensitive operations. SIF retrieval using the in-filling of solar Fraunhofer lines has an advantage since the spectral structure of solar Fraunhofer lines is not modified by atmospheric phenomena and aerosols as is the case with atmospheric oxygen absorption features (Joiner et al., 2011; Frankenberg et al., 2011, Joiner et al., 2011). Consequently, the hyper-spectral system can detect SIF despite cloudy conditions.

The stability of the hyper-spectral system and the use of Fraunhofer line in-filling allows for the use of a fast near least square fit approach to determine the SIF signal. The spectral fitting method selected applies the least square retrieval approach for the standard analysis. Future investigations will reveal if the conclusion remains valid for long-term datasets.

The system employs a newly developed RotaPrism, which was designed to provide spatial canopy scans and probe various plants with a single instrument. A special feature of the RotaPrism is that it can take simultaneous co-centered observations of surface reflectance, spectral albedo, and SIF. The spatial scanning strategies can help investigate various questions on the

interpretation and use of SIF. These questions include the behavior of individual plant species, the impact of radiative transfer conditions in the canopy on SIF.

The fluxtower-based hyper-spectral observations will provide unique continuous datasets on photosynthetic activity in a natural and agricultural ecosystem with high temporal resolution, thereby bridging the gap between leaf, canopy, and satellite SIF observations. The data will allow for the investigation of the impact of environmental stress on photosynthetic processes and CO₂ exchange.

Bibliography

- Allen, W. A., et al. (1970). "Plant–canopy irradiance specified by the Duntley equations." *JOSA* 60(3): 372–376.
- Allen, W. A. and A. J. Richardson (1968). "Interaction of light with a plant canopy." *JOSA* 58(8): 1023–1028.
- Barducci, A., et al. (2009). "Investigating the angular and spectral properties of natural targets using CHRIS-PROBA images of San Rossore test site." *International Journal of Remote Sensing* 30(3): 533–553.
- Billings, W., et al. (1961). "Effect of low concentrations of carbon dioxide on photosynthesis rates of two races of *Oxyria*." *Science* 133(3467): 1834–1834.
- Björkman, O. (1966). "The effect of oxygen concentration on photosynthesis in higher plants." *Physiologia Plantarum* 19(3): 618–633.
- Björkman, O. and P. Holmgren (1963). "Adaptability of the photosynthetic apparatus to light intensity in ecotypes from exposed and shaded habitats." *Physiologia Plantarum* 16(4): 889–914.
- Carlson, T. N. and D. A. Ripley (1997). "On the relation between NDVI, fractional vegetation cover, and leaf area index." *Remote sensing of environment* 62(3): 241–252.
- Cheng, Y.–B., et al. (2013). "Integrating solar induced fluorescence and the photochemical reflectance index for estimating gross

primary production in a cornfield." *Remote Sensing* 5(12): 6857–6879.

Chisholm, L., et al. (2015). "The spectroscopy dataset lifecycle: Best practice for exchange and dissemination."

Cogliati, S., et al. (2015). "Continuous and long-term measurements of reflectance and sun-induced chlorophyll fluorescence by using novel automated field spectroscopy systems." *Remote sensing of environment* 164: 270–281.

Drolet, G. G., et al. (2005). "A MODIS-derived photochemical reflectance index to detect inter-annual variations in the photosynthetic light-use efficiency of a boreal deciduous forest." *Remote sensing of environment* 98(2–3): 212–224.

Feret, J.-B., et al. (2008). "PROSPECT-4 and 5: Advances in the leaf optical properties model separating photosynthetic pigments." *Remote sensing of environment* 112(6): 3030–3043.

Féret, J.-B., et al. (2017). "PROSPECT-D: Towards modeling leaf optical properties through a complete lifecycle." *Remote sensing of environment* 193: 204–215.

Floridi, L. (2005). "Is semantic information meaningful data?" *Philosophy and phenomenological research* 70(2): 351–370.

Fratini, G., et al. (2012). "Relative humidity effects on water vapour fluxes measured with closed-path eddy-covariance systems with short sampling lines." *Agricultural and forest meteorology* 165: 53–63.

Gabrielsen, E. (1949). "Photosynthesis in leaves at very low carbon dioxide concentrations." *Nature* 163(4140): 359–360.

- Gamon, J., et al. (1992). "A narrow-waveband spectral index that tracks diurnal changes in photosynthetic efficiency." *Remote sensing of environment* 41(1): 35–44.
- Gitelson, A. A., et al. (2006). "Three-band model for noninvasive estimation of chlorophyll, carotenoids, and anthocyanin contents in higher plant leaves." *Geophysical research letters* 33(11).
- Gu, L., et al. (2005). "Objective threshold determination for nighttime eddy flux filtering." *Agricultural and forest meteorology* 128(3–4): 179–197.
- Gu, L., et al. (2019). "Advancing terrestrial ecosystem science with a novel automated measurement system for sun-induced chlorophyll fluorescence for integration with eddy covariance flux networks." *Journal of Geophysical Research: Biogeosciences* 124(1): 127–146.
- Hall, F. G., et al. (2008). "Multi-angle remote sensing of forest light use efficiency by observing PRI variation with canopy shadow fraction." *Remote sensing of environment* 112(7): 3201–3211.
- Hilker, T., et al. (2009). "An assessment of photosynthetic light use efficiency from space: Modeling the atmospheric and directional impacts on PRI reflectance." *Remote sensing of environment* 113(11): 2463–2475.
- Horst, T. and D. Lenschow (2009). "Attenuation of scalar fluxes measured with spatially-displaced sensors." *Boundary-layer meteorology* 130(2): 275–300.
- Huete, A., et al. (1997). "A comparison of vegetation indices over a global set of TM images for EOS-MODIS." *Remote sensing of environment* 59(3): 440–451.
- Jacquemoud, S. and F. Baret (1990). "PROSPECT: A model of leaf

optical properties spectra." *Remote sensing of environment* 34(2): 75–91.

Jong–Hwan, L., et al. (2003). "Forest stand structure, site characteristics and carbon budget of the Kwangneung natural forest in Korea." *Korean Journal of Agricultural and Forest Meteorology* 5(2): 101–109.

Kang, M., et al. (2018). "Changes and improvements of the standardized eddy covariance data processing in KoFlux." *Korean Journal of Agricultural and Forest Meteorology* 20(1): 5–17.

Kang, M., et al. (2009). "Evapotranspiration from a deciduous forest in a complex terrain and a heterogeneous farmland under monsoon climate." *Asia–Pacific Journal of Atmospheric Sciences* 45(2): 175–191.

Kim, J., et al. (2006). "HydroKorea and CarboKorea: cross–scale studies of ecohydrology and biogeochemistry in a heterogeneous and complex forest catchment of Korea." *Ecological Research* 21(6): 881–889.

Kubelka, P. and F. Munk (1931). "An article on optics of paint layers." *Z. Tech. Phys* 12(593–601): 259–274.

Lee, J.–E., et al. (2013). "Forest productivity and water stress in Amazonia: Observations from GOSAT chlorophyll fluorescence." *Proceedings of the Royal Society B: Biological Sciences* 280(1761): 20130171.

Liu, X. and L. Liu (2018). "Influence of the canopy BRDF characteristics and illumination conditions on the retrieval of solar–induced chlorophyll fluorescence." *International Journal of Remote Sensing* 39(6): 1782–1799.

Magney, T. S., et al. (2016). "Response of high frequency Photochemical Reflectance Index (PRI) measurements to environmental conditions in wheat." *Remote sensing of environment* 173: 84–97.

Mazzoni, M., et al. (2012). "Retrieval of maize canopy fluorescence and reflectance by spectral fitting in the O₂-A absorption band." *Remote sensing of environment* 124: 72–82.

McAlister, E. D. and J. Myers (1940). "The time course of photosynthesis and fluorescence observed simultaneously." *Smithsonian Miscellaneous Collections*.

Middleton, E., et al. (2009). Diurnal and seasonal dynamics of canopy-level solar-induced chlorophyll fluorescence and spectral reflectance indices in a cornfield. *Proceedings, 6th EARSeL SIG Workshop on Imaging Spectroscopy, CD-ROM*.

Penndorf, R. (1956). "Colors of natural objects." *JOSA* 46(3): 180–182.

Porcar-Castell, A., et al. (2014). "Linking chlorophyll a fluorescence to photosynthesis for remote sensing applications: mechanisms and challenges." *Journal of experimental botany* 65(15): 4065–4095.

Rascher, U., et al. (2015). "Sun-induced fluorescence—a new probe of photosynthesis: First maps from the imaging spectrometer HyPlant." *Global change biology* 21(12): 4673–4684.

Reichstein, M., et al. (2005). "On the separation of net ecosystem exchange into assimilation and ecosystem respiration: review and improved algorithm." *Global change biology* 11(9): 1424–1439.

Rocha, A. V. and G. R. Shaver (2011). "Burn severity influences

postfire CO₂ exchange in arctic tundra." *Ecological applications* 21(2): 477–489.

Rowley, J. (2007). "The wisdom hierarchy: representations of the DIKW hierarchy." *Journal of information science* 33(2): 163–180.

Sabater, N., et al. (2018). "Compensation of oxygen transmittance effects for proximal sensing retrieval of canopy-leaving sun-induced chlorophyll fluorescence." *Remote Sensing* 10(10): 1551.

Schulze, E.-D. (1966). *Wintertime Photosynthesis on Bristlecone Pine in the White Mountains of California*, University of California, Los Angeles–Botany.

Serbin, S. P., et al. (2012). "Leaf optical properties reflect variation in photosynthetic metabolism and its sensitivity to temperature." *Journal of experimental botany* 63(1): 489–502.

Sims, D. A. and J. A. Gamon (2002). "Relationships between leaf pigment content and spectral reflectance across a wide range of species, leaf structures and developmental stages." *Remote sensing of environment* 81(2–3): 337–354.

Strub, G., et al. (2003). "Evaluation of spectrodirectional Alfalfa canopy data acquired during DAISEX'99." *IEEE Transactions on Geoscience and Remote Sensing* 41(5): 1034–1042.

Suits, G. H. (1971). "The calculation of the directional reflectance of a vegetative canopy." *Remote sensing of environment* 2: 117–125.

Tan, B., et al. (2006). "The impact of gridding artifacts on the local spatial properties of MODIS data: Implications for validation, compositing, and band-to-band registration across resolutions." *Remote sensing of environment* 105(2): 98–114.

- Tucker, C. J. (1979). "Red and photographic infrared linear combinations for monitoring vegetation." *Remote sensing of environment* 8(2): 127–150.
- van Gorsel, E., et al. (2009). "Estimating nocturnal ecosystem respiration from the vertical turbulent flux and change in storage of CO₂." *Agricultural and forest meteorology* 149(11): 1919–1930.
- van Gorsel, E., et al. (2008). "Application of an alternative method to derive reliable estimates of nighttime respiration from eddy covariance measurements in moderately complex topography." *Agricultural and forest meteorology* 148(6–7): 1174–1180.
- Van Gorsel, E., et al. (2007). "Nocturnal carbon efflux: reconciliation of eddy covariance and chamber measurements using an alternative to the u_z-threshold filtering technique." *Tellus B: Chemical and Physical Meteorology* 59(3): 397–403.
- Verhoef, W. (1984). "Light scattering by leaf layers with application to canopy reflectance modeling: The SAIL model." *Remote sensing of environment* 16(2): 125–141.
- Vilfan, N., et al. (2016). "Fluspect-B: A model for leaf fluorescence, reflectance and transmittance spectra." *Remote sensing of environment* 186: 596–615.
- Webb, E. K., et al. (1980). "Correction of flux measurements for density effects due to heat and water vapour transfer." *Quarterly Journal of the Royal Meteorological Society* 106(447): 85–100.
- Wilczak, J. M., et al. (2001). "Sonic anemometer tilt correction algorithms." *Boundary-layer meteorology* 99(1): 127–150.
- Wong, C. Y. and J. A. Gamon (2015). "Three causes of variation in

the photochemical reflectance index (PRI) in evergreen conifers."
New Phytologist 206(1): 187–195.

Zhang, Q., et al. (2019). "Comparison of Bi-hemispherical and hemispherical-conical configurations for in situ measurements of solar-induced chlorophyll fluorescence." Remote Sensing 11 (22): 2642.

Abstract

초 분광 원격 감지는 식생 구조와 기능을 모니터링하는 강력한 도구가 되고 있다. 특히, 식물의 생리적, 구조적 변화를 이해하기 위해 태양광 유도 엽록소 형광 (SIF)과 캐노피 반사율 모니터링이 널리 이용되고 있다. 현장 분광법은 높은 스펙트럼, 시간 분해능 현장 데이터를 제공하고 작은 영역에서 큰 영역으로 측정을 확장하는 수단을 제공하기 위한 중요한 기술로 확립되었다. 그러나, 수많은 연구가 현장 분광 시스템을 개발했지만, 반구-원추형 및 양 반구 구성 간의 원격 감지 관찰의 기하학적 및 광학적 차이에 대한 이해가 부족할 뿐만 아니라 초 분광 데이터를 지속적으로 수집하는 것은 여전히 어렵다.

우리는 반구형-원추형 및 이중 반구형 구성으로 원격외선 태양광 유도 엽록소 형광 및 캐노피 초 분광 반사율(400-900nm)을 측정하는 자동화된 지상 기반 필드 분광 시스템을 개발했다. 양방향 반사율과 반구형 원추형 반사율을 모두 측정하기 위해 서보 모터를 사용하여 프리즘을 회전하여 세가지 타입의 포트를 측정한다. 각 포트는 들어오는 복사 조도, 나가는 복사 조도 및 나가는 복사를 측정하는 세 가지 유형의 포트다. 조사조도는 백색확산유리와 굴절 렌즈를 사용하였고, 굴절 렌즈를 이용하여 조도를 측정하였다. 또한, 우리는 방사 측정 및 과장 교정을 포함하는 데이터 관리 프로토콜을 개발했다. 마지막으로, 우리는 낙엽 활엽수림의 성장기에 이 시스템에서 측정된 BRF와 BHR 데이터가 어떻게 다른지 보고하였다.